ISSN 1392–1320 MATERIALS SCIENCE (MEDŽIAGOTYRA). Vol. 29, No. 1. 2023

Experimental Investigation on Evaporator Surface Modification for Hydrophobicity and Frost Resistance

Xingyuan LIANG, Lijun WU *, Zengzhi WEI

School of Mechanical Engineering, Tongji University, Shanghai 201804, PR China

crossref http://dx.doi.org/10.5755/j02.ms.30986

Received 28 March 2022; accepted 16 May 2022

Frost accumulated on the surface of the evaporator leads to the increase of heat transfer resistance between the refrigerant and environmental medium, which reduces the system performance of cold storage and air source heat pump. To solve this problem, the surface-modified evaporator can achieve retardation of the frost formation, which greatly improves the heat exchange effect between the refrigerant and the external environment. In this paper, a novel coating sprayed on the evaporator was developed using the sol-gel method and the hydrophobicity, durability, and thermal conductivity were investigated. Moreover, a modified method of frost weight measurement under different temperatures and humidity was first proposed. The results showed that the coating has a favorable hydrophobic effect and thermal conductivity, and long service life. Under the standard experimental condition, the frost weight on the coating surface can be reduced up to 26.1 %. Additionally, the effect of coating composition ratio on its performance was further investigated. To sum up, this new coating has the potential for industrialized application.

Keywords: hydrophobic coating, frost retardation, frost measurement, poly tetrafluoroethylene, variance analysis.

1. INTRODUCTION

Frost is a common phenomenon. When moist air flows through the surface below both the dew point and the freezing point of the air, the surface of the evaporator will frost [1, 2]. Based on the knowledge of heat transfer, the heat transfer resistance between the frost layer and external environment is increased when the frost layer accumulates on the surface of the evaporator 3. Specifically, for the cold storage system, evaporator frost leads to food corruption, and the breeding of bacteria in the storage 4, and for the air source heat pump will increase its energy consumption [5, 6]. Therefore, frost formation has aroused the broad interest of researchers [7, 8].

There are active and passive methods to restrain surface frosting. Active methods include preheating 9 and dehumidifying [10, 11] moist air, external electric field 12 and magnetic field 13. Although active methods can delay frosting in most conditions, additional devices need to be added to implement these methods. Therefore, the initial investment cost and power consumption are increased, and the effect on improving energy efficiency is limited 14. Passive methods, including redesigning the heat exchanger structure 15, adjusting fin shape 16 and spacing 17, are often used to suppress frosting only under specific conditions and the effect is limited. Based on the problems of the above methods, using a hydrophobic coating to modify the evaporator surface has unique advantages, including no extra energy consumption, the system's complexity does not change, and is widely applicable to frosting conditions [18, 19].

The hydrophobic surface can be fabricated by coating a water-repellent material or etching the surface [20, 21]. Nevertheless, the etching method was used on small flat experimental surfaces, nearly impossible to be applied to the heat exchanger surface fabrication due to the complicated process [22, 24]. In the early stage, automobile wax containing silicone was coated on the bare surface with 90 – 100° or Teflon emulsion was sprayed on the aluminum alloy surface with 100 – 110° water contact angle (WCA) [25, 26]. Later, the $Al(OH)_3$ nanostructure was induced by alkali-treatment on the surface of aluminum alloy, and the self-assembled superhydrophobic surface was obtained by Kim et al 27. The surface WCA of the coating is up to 165°, and the frosting test proves that the coating has good frost retardation performance. However, the whole specimen shall be immersed in boiling deionized water for 30 min to form nanostructures. A ZrO_2-incorporated fluoropolymer coating with 153° WCA was prepared by Kulinich et al 28, which has a similar problem in the complex fabrication process. The suspension and substrate shall be in a rotating machine, with the substrate rotating, the suspension adhered to it, and the frost restrains effect was not significant. It seems a kind of frost retardation coating with an easily prepared process that can be directly adhered to the existing heat exchanger is required. And the hydrophobicity of Teflon emulsion needs to be improved by other additives.

PTFE($(CF_2CF_2)_n$), also called Teflon, has exceptional heat resistance, low-temperature resistance, self-lubrication and chemical stability and is widely used in non-stick stainless pans. Teflon has been used to establish the superhydrophobic property of the surface [29, 30].

* Corresponding author. Tel.: +86-13917547917.
E-mail address: *ljwu@tongji.edu.cn* (L. Wu)

Nanoscale silica can significantly improve surface roughness and reduce surface energy, which helps to improve the WCA [31, 32]. Many methods have been reported to fabricate self-cleaning multifunctional coatings containing nano SiO_2 and TiO_2, including the double or multi-layer structure of high WCA index by using sol-gel preparation methods [33 – 35]. The primary material of the evaporator is type 304 stainless steel, which as a metal has more favorable thermal conductivity than coating. So nanometer graphite powder was also reinforced to improve the thermal conductivity for our coating [36, 37]. SiO_2 is hydrophilic, without treatment to fill the hydrophobic PTFE, due to the interface between SiO_2 and PTFE is very difficult to form a chemical bond, resulting in poor compatibility between the two phases, which means high porosity and water uptake in humid environments, and poor mechanical integrity [38, 39], so the selection of appropriate coupling agent is conducive to the bonding effect between the polymer and SiO_2. Aminopropyltriethoxysilane(KH550, $NH_2(CH_2)_3Si(OC_2H_5)_3$) contributes to the hydrophobic effect of the combination of SiO_2 and PTFE, decreases the porosity and moisture absorption, also increases density [40, 41]. Meanwhile, adding KH550 can improve interfacial adhesion, higher thermal conductivity and lower in-plane orientation degree than PTFE without KH550 42. Going through these researches above, PTFE, nanoscale silica, nanoscale graphite powder, titanium dioxide and silane coupling agent were selected to prepare this coating.

In addition, a modification method for frost weight measurement under different temperature and humidity conditions was first proposed in this paper to cope with the influence of the disunity of temperature and humidity conditions on the frost weight measurement. Furthermore, the effect of each component on the properties of the coating was analyzed based on the measurement of surface frosting weight, thermal conductivity and other indexes.

2. EXPERIMENT

2.1. Theory of hydrophobicity and retard frost formation

Frost is the phase transition of water vapor in moist air, contacting a cold surface. It is closely related to surface properties because phase nucleation requires overcoming the Gibbs free energy barrier 43. A larger WCA of the solid surface required a higher Gibbs free energy barrier during the embryo formation process [25, 44].

ΔG_c is the critical Gibbs energy change at critical embryo size:

$$\Delta G_{\mathrm{c}} = \frac{16\pi}{3}\frac{\sigma_{\mathrm{ij}}^3}{\Delta g_{\mathrm{v}}^2} f(\theta) = \frac{4\pi}{3}\frac{\sigma_{\mathrm{ij}}^3}{\Delta g_{\mathrm{v}}^2}[(\cos\theta)^3 - 3\cos\theta + 2], \quad (1)$$

where σ_{ij} is the interfacial energy; Δg_{v} is the specific Gibbs energy change; θ is the WCA. In this equation, the critical Gibbs energy change ΔG_{c} is a monotonically increasing function of WCA θ 45. The embryo formation rate I in a unit surface for heterogeneous nucleation depends on the critical Gibbs energy change ΔG_{c}, viz.

$$I = I_0 \cdot \exp\left(-\frac{\Delta G_{\mathrm{c}}}{k \cdot T_k}\right), \quad (2)$$

where I_0 is the kinetic constant; k is the Boltzmann constant; T_{k} is the surface temperature. This formula indicates that the larger ΔG_c is, the smaller embryo formation rate I is, which means a slower frost formation rate.

Furthermore, when the frost melting mechanism is considered, the hydrophobic surface is more likely to make the frost that melts into water fall off. Kim et al 46. deduced the radius of departure drops from the capillary force and gravity balance, viz.

$$r_{\max} = \left[\frac{6c(\cos\theta_{\mathrm{r}} - \cos\theta_{\mathrm{a}})\sin\theta}{\pi(\cos^3\theta - 3\cos\theta + 2)} \cdot \frac{\sigma}{\rho g}\right]^{1/2}, \quad (3)$$

The first fraction on the right side is reduced as θ increases, which means a more extensive contact angle will reduce the radius of departure drops and makes the hydrophobic surface defrosting more efficient than the surface not modified.

2.1. Preparation of PTFE hydrophobic frost retardation coating

In the introduction chapter, the materials used to prepare the coating are shown, and the specific manufacturing steps are described in Fig. 1.

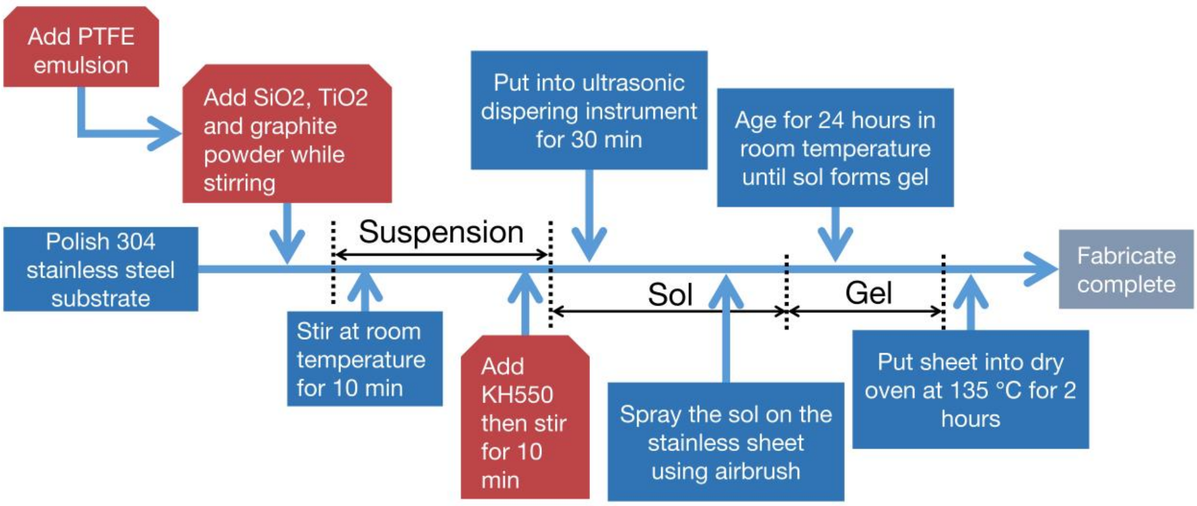

Fig. 1. The sol-gel process of preparation the hydrophobic frost retardation coating

First, the stainless steel surface as the substrate was polished with emery paper to remove the dirt and oxide on the surface. Polish also improved the roughness of the substrate to enhance the bonding strength of the coating and the substrate. PTFE emulsion (PTFE particle wt = 30 %, fluorocarbon emulsion wt = 70 %, Dongguan Zhanyang polymer materials Co., Ltd.) was added first, then fumed SiO_2 (20 nm, Shaoxing Lijie Chemical Co., Ltd); TiO_2 (> 98 %, Sinopharm Chemical Reagent Co., Ltd) and graphite powder (> 98 %, Sinopharm Chemical Reagent Co., Ltd) were put into glass flask sequentially while they were all magnetic stirred, and the contents of each component are shown in Table 1. After stirring for 10 min, KH550 (Jinan Xingfeilong Chemical Co., Ltd.) shall be poured in and stirred for another 10 min at room temperature to form an organic-inorganic hybrid. The suspension was formed by stirring and then was put into an ultrasonic dispersing instrument for 30 min dispersion and became to sol. Next, the sol was sprayed on the stainless sheet with an airbrush. The sol on the stainless sheet was aged for 24 hours at room temperature until it was dry and became to gel. Putting the sheet into the drying oven at 135 ℃ for 2 hours to remove residual moisture and the coating on the stainless sheet was finished. Different material ratios for other groups were processed in the same process as above.

The coating preparation method is simple and with few steps. In particular, the coating can be directly sprayed on the surface of the existing evaporator using a spray gun, which has a favourable industrial application prospect.

An orthogonal experiment was carried out to find out the influence of each ingredient on the properties of the coating. The orthogonal experiment uses an orthogonal table to design multi-factor and multi-level tests and is often used in process analysis and optimization because it can comprehensively cover the selected experimental range while saving cost [47, 48]. According to the preparation of the preliminary experiment, based on 20 g PTFE, we have obtained the approximate range of each ingredient. Due to SiO_2 having a significant impact on the WCA, an extra level was considered. A $L_{12}(4^1 \times 3^3)$ orthogonal experiment table was given in Table 1. The range has been confirmed in preliminary preparation work to prepare the coating successfully, which SiO_2 is 0.4 – 2.5/g, TiO_2 is 0.5 – 1.2/g, C is 0.6 – 1/g, KH550 is 0.1 – 1/g. In these ranges, the coating prepared by different values has slightly different properties. All 14 orthogonal experiment samples were fabricated and showed in Fig. 2.

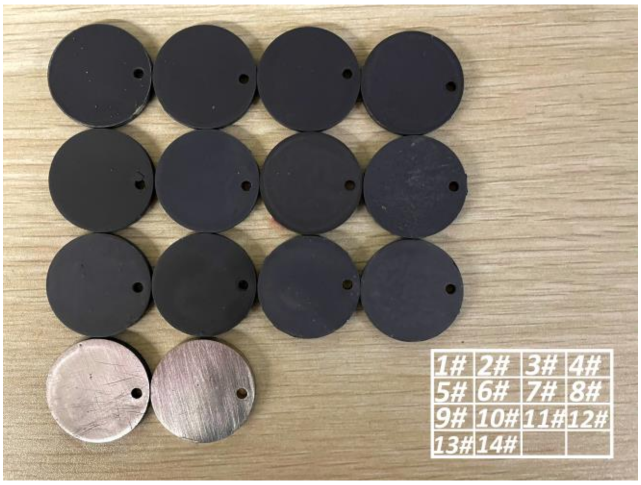

Fig. 2. The sample of 14 experimental sheets

Table. 1. $L_{12}(4^1 \times 3^3)$ orthogonal experiment table

Factor	Level			
	1	2	3	4
SiO2/g	A	B	C	D
TiO2/g	A	B	C	/
C/g	A	B	C	/
KH550/g	A	B	C	/
Note: A, B, C, D all represent a specific value within the corresponding range.				

Table 2. Orthogonal experiment and results

No.	PTFE, g	SiO_2, g	TiO_2, g	C, g	KH550, g	Temperature, ℃	Relativity humidity, %	15 min frost weight, g	Frost weight in standard condition, g	WCA, °	Thermal conductivity, $W(m \times K)^{-1}$	WCA degradation, °
1#	20	A	A	A	B	19	67	0.093	9.144E-02	105.2	1.18	5.5
2#	20	A	B	B	C	20	58	0.087	9.300E-02	104.9	1.76	2
3#	20	A	C	C	A	19	66	0.096	9.582E-02	104.4	2.96	5.1
4#	20	B	A	B	A	20	57	0.081	8.811E-02	111.9	0.77	8.1
5#	20	B	B	C	B	20	58	0.085	9.086E-02	110.6	2.75	8.4
6#	20	B	C	A	C	19	66	0.095	9.482E-02	115	1.53	1.4
7#	20	C	A	C	C	20	58	0.069	7.376E-02	143.9	2.27	22.7
8#	20	C	B	A	A	19	61	0.078	8.423E-02	125.3	0.63	8.8
9#	20	C	C	B	B	19	60	0.068	7.466E-02	140.4	1.72	5.3
10#	20	D	A	C	C	20	59	0.072	7.566E-02	143.9	1.54	12.1
11#	20	D	B	A	A	20	68	0.092	8.388E-02	145.8	0.46	9.7
12#	20	D	C	B	B	20	63	0.086	8.463E-02	142.9	0.87	8.3
13#	20	0	0	0	0	19	66	0.097	9.682E-02	99.4	0.11	7
14#	0	0	0	0	0	19	66	0.100	9.981E-02	72.9	11.30	
Note: 13# is pure PTFE coating and 14# is bare stainless sheet.												

2.3. Coating properties tests and methods

Water contact angle measurement and shooting instrument (Guangdong Aisirui Instrument Technology Co., Ltd.) was applied to measure the WCA. For each test 0.05ml water was dropped on the coating surface. Two sheets were prepared for WCA and performance degradation measurement. Each sheet measured WCA seven times in different places on its surface. WCA value was the average of these 14 times measurements. Due to the WCA of the overall sheet was not uniform, in those better hydrophobic sheets, some sampling points can reach superhydrophobicity. With further research, superhydrophobic coatings with an average WCA higher than 150° can be prepared by this method.

A semiconductor refrigeration frosting system (HKJ-CL50, Jiumu Tongda (Linyi) Refrigeration Technology Co., Ltd.) is shown in Fig. 3. It could decrease the temperature of the semiconductor chilling plate surface to -25 °C, and experimental samples were placed on it to frost. Frost weight was measured with an electronic balance with an accuracy of ten thousandths in a gram. However, the frost weight is seriously affected by indoor temperature and humidity. During the experiment, the temperature and humidity were slightly changed. So the actual frost weight shall be converted to the frost weight at 20 °C and 62 % relative humidity, which was the most common condition in our lab. This modified method of frost weight measurement under different temperature and humidity environments was first proposed as described below.

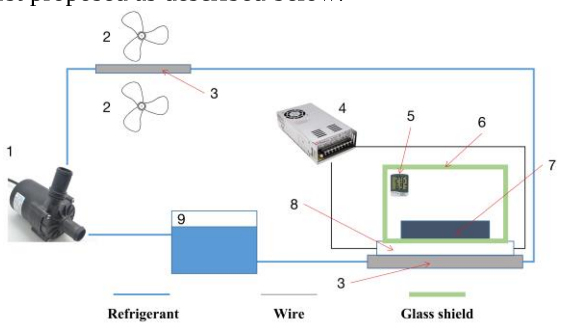

Fig. 3. Schematic diagram of semiconductor refrigeration frosting system: 1 – small water pump; 2 – fans; 3 – refrigerant block; 4 – switching power supply; 5 – hygrothermograph; 6 – glass shield; 7 – test samples; 8 – semiconductor chilling plate; 9 – regfrigerant tank

Assumed that the actual amount of water vapor in the moist air is proportional to the frost weight form on the cold surface, viz.

$$d = km_V = k\varphi m, \tag{4}$$

where d is the frost weight; k is proportionality factor; m_V is the actual amount of water vapor in moist air. And cconsidering the definition of relative humidity; φ is relative humidity and m is the mass of water vapor in saturated wet air at the same temperature and total pressure.

The subscript stand is a standard condition, the act is actual experimental condition. Simultaneous the equations in both standard condition and actual experimental condition, viz.

$$d_{\text{stand}} = d_{\text{act}} \frac{\varphi_{\text{stand}}}{\varphi_{\text{act}}} \frac{m_{\text{stand}}}{m_{\text{act}}} = d_{\text{act}} \frac{\varphi_{\text{stand}}}{\varphi_{\text{act}}} \frac{p_{s\text{stand}}}{p_{s\text{act}}}, \tag{5}$$

where p_s is the partial pressure of water vapor in saturated wet air at the same temperature and total pressure; p_s shall be looked up in saturated air's state parameters at the 0.1 MPa table 49. Frost weight in this paper was all converted to the standard experimental condition in this method and can be regarded as the evaluation index of frost retardation.

Considering frost weight was influenced by temperature and humidity, the condensation may occur on the surface of the frosted sample during weighing. The samples were weighed as soon and precise as possible, but the error of frost weight shall also be calculated. The error transfer formula used to calculate the error transfer of the corresponding relative error is 50:

$$\frac{\Delta y}{y} = \frac{1}{y}\left[\sum_{i=1}^{n}\left(\frac{\partial f}{\partial x_i}\Delta x_i\right)^2\right]^{\frac{1}{2}}, \tag{6}$$

where Δx_i is the absolute error of direct measurement parameter x_i, Δy is the absolute error of indirect measurement parameter caused by Δx_i, f is the functional relationship between indirect and direct measurement parameters. $\frac{\partial f}{\partial x_i}$ is the error transfer coefficient. The frost weight d_{satnd} was considered.

$$\frac{\Delta d_{\text{stand}}}{d_{\text{stand}}} = \frac{\varphi_{\text{act}} p_{s\text{act}}}{d_{\text{act}}}\left[\left(\frac{\Delta t_{\text{act}}}{p_{s\text{act}}\varphi_{\text{act}}}\right)^2 + \left(\frac{d_{\text{act}}\Delta\varphi_{\text{act}}}{p_{s\text{act}}\varphi_{\text{act}}}\right)^2 \left(\frac{d_{\text{act}}\Delta p_{s\text{act}}}{p_{s\text{act}}\varphi_{\text{act}}}\right)^2\right]^{\frac{1}{2}}, \tag{7}$$

The accuracy of the electronic balance and relative humidity are $\pm 5 \times 10^{-4}$ g and ± 1 %. The accuracy of temperature is ± 0.5 °C, so the ± 0.5 °C can cause ± 0.0772 kPa in the partial pressure of water vapor in saturated wet air p_s within the experimental temperature range. Now put 6# and 12# data in Eq. 7, the relative error of d_{satnd} is 5.4 % and 5.3 %. Measurement error also was considered in variance analysis to exclude its influence. So in the experiment process, the range of measurement error was supposed to be acceptable.

Based on the transient hot-wire method, the thermal conductivity of the coating and stainless steel substrate as an entirety can be measured. Applied the simple heat transfer knowledge 51, the thermal conductivity of coating was calculated, viz.

$$\lambda_1 = \frac{\lambda\delta_1\lambda_2}{(\delta_1+\delta_2)\lambda_2-\delta_2\lambda}, \tag{8}$$

where λ_1 is the thermal conductivity of coating; λ_2 is the thermal conductivity of stainless steel substrate, which can get from sample14#, λ is the result of transient hot-wire method; t_1 and t_2 is the temperature of the upper and lower surfaces of the experimental sample; δ_1 and δ_2 is the thickness of coating and substrate.

3. RESULTS AND DISCUSSION

3.1. Frost retardation, thermal conductivity and performance degradation of WCA

Fig. 4 shows the frost weight at different WCA during the experiment time. From the chart, in the beginning, the WCA seems not to affect the frost weight. This phenomenon is because the surface has not been wholly cooled at the beginning of the experiment, resulting in surface frosting only in the edge area, while the frosting in the center area of the surface is limited, so the frost weight has little relationship with the surface WCA.

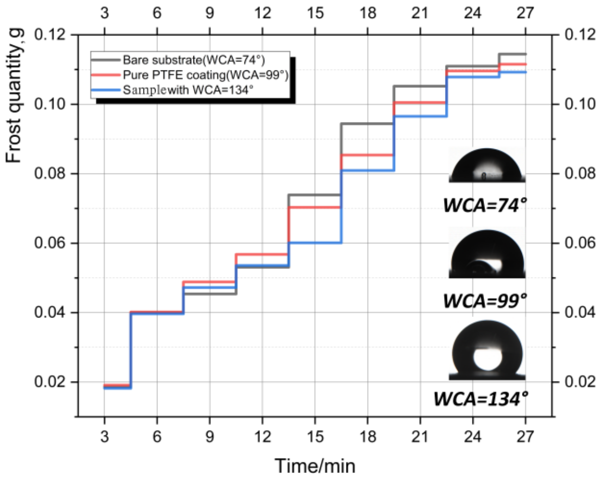

Fig. 4. The curve of frost weight with time at different WCA

Frost weight converges finally after 24 – 27 min, for which Kim et al. 8 summarized that the surface properties only affected the dry face to the formation of ice crystals and could not influence the frost layer's growth. In other words, the surface coating can not be completely anti-frosting. The purpose of surface modification is retarding the frost formation, and the other is facilitating water drainage and frost removal to improve defrosting [7]. Due to the easy installment, defrosting techniques, such as an electric heater on a heat exchanger, should also be utilized [52, 53]. The frost measurement time for this paper shall be between 15 – 18 min. Consider at 15 min, and the frost weight has more significant difference between WCA = 99°, 135°; 15 min was settled to measure frost weight in the discussion of coating composition ratio on its performance.

From Table 2, the 15 min frost weight in standard condition for 12 groups of coating is 4.00 – 26.10 % lower than the bare stainless substrate and 2.00 – 22.89 % lower than pure PTFE coating. This coating shows a pretty good frost retardation effect.

In Fig. 5, the thermal conductivity of the coating is indeed much lower than that of the integral sheet. However, due to the nanoscale graphite powder, all coatings have better thermal conductivity than pure PTFE coating. Nevertheless, the measurement results of the integral sheets are 4.47 – 19.17 % lower than the substrate. The coating affects frost retardation, which offsets the thermal resistance of frost. The decrease of thermal conductivity for the integral sheet can be acceptable.

Fig. 6 shows the degradation of WCA, and it can be seen that the degradation has some fluctuations although the tendency decreases. Because the WCA measurement points on coating can not be precisely the same and the coating is not entirely uniform. To analyze the performance degradation here, Δθ was used, viz.

$$\Delta\theta = \theta_{\mathrm{Day1}} + \theta_{\mathrm{Day6}} + \theta_{\mathrm{Day11}} - \theta_{\mathrm{Day21}} - \theta_{\mathrm{Day27}} - \theta_{\mathrm{Day31}}. \tag{9}$$

Now, frost measurement time and the WCA performance degradation method have been ensured. A $L_{12}(4^1\times3^3)$ orthogonal experiment can be carried out, and all experimental data are shown in Table 2. Total 14 experiments were done and exhibited in Fig. 2, besides 13# was pure PTFE coating and 14# was polished bare stainless sheets.

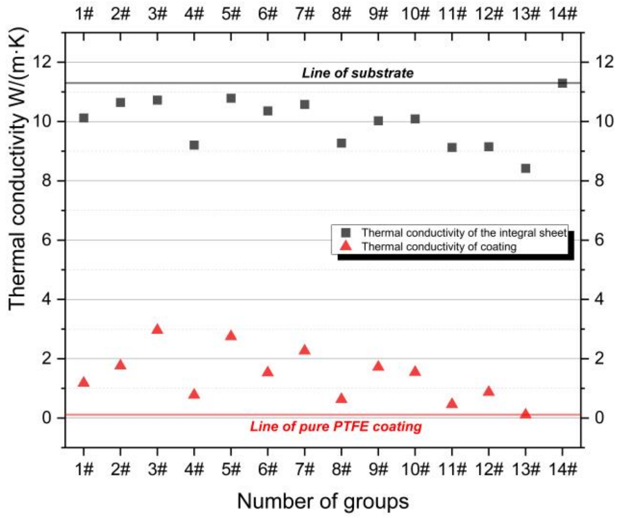

Fig. 5. Thermal conductivity of integral sheet and coating

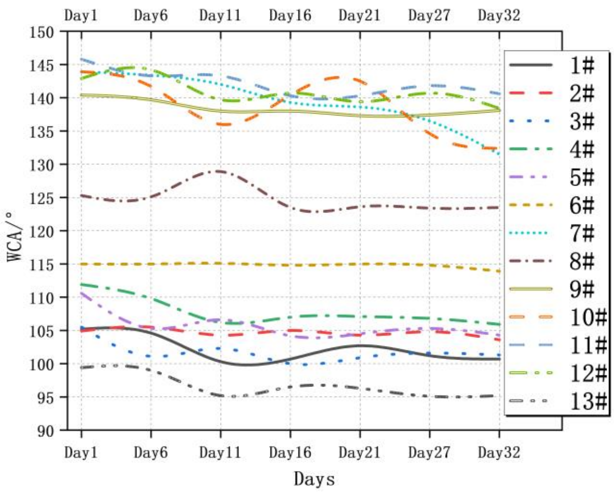

Fig. 6. The change of WCA for 13 samples during experimental days (13# is the pure PTFE coating)

3.2. Extreme difference analysis and variance analysis

3.2.1. Calculation process

With the help of the extreme difference analysis(EDA) and variance analysis(VA), the effects of silicon dioxide (SiO_2); titanium dioxide (TiO_2); graphite powder (C); poly tetra fluoroethylene (PTFE) and aminopropyltriethoxysilane (KH550) on hydrophobic property; frost retardation; heat transfer characteristic and performance degradation were discussed. The progress of EDA does not need to explain and the results of EDA are shown below.

Table. 3. Results of EDA

Index	WCA θ, °				Frost weight in standard condition d_{stand}, g				Thermal conductivity λ_1, $W(m\times K)^{-1}$				WCA degradation $\Delta\theta$, °			
	SiO_2	TiO_2	C	KH550	SiO_2	TiO_2	C	KH550	SiO_2	TiO_2	C	KH550	SiO_2	TiO_2	C	KH550
$\overline{K_{i1}}$	104.83	126.23	122.83	121.85	0.0934	0.0822	0.0886	0.0880	1.97	1.44	0.95	1.21	4.20	12.10	6.35	7.92
$\overline{K_{i2}}$	112.50	121.65	125.03	124.78	0.0913	0.0880	0.0851	0.0854	1.68	1.40	1.28	1.63	5.97	7.22	5.93	6.87
$\overline{K_{i3}}$	136.53	125.68	125.70	126.93	0.0776	0.0875	0.0840	0.0843	1.54	1.77	2.38	1.78	12.27	5.02	12.08	9.55
$\overline{K_{i4}}$	144.20	–	–	–	0.0814	–	–	–	0.96	–	–	–	10.03	–	–	–
R_i	39.37	4.57	2.87	5.08	0.0159	0.0058	0.0046	0.0037	1.01	0.37	1.43	0.57	8.07	7.08	6.15	2.68
Note: the factors which have the biggest influence on its experimental item have a dotted background in this table.																

The progress of VA shall be explained briefly [54-55]. The sum of corresponding trial index for each level k of factor i (i = 1, 2, 3, 4; k = 1, 2, 3 (for SiO_2 k = 1, 2, 3, 4)) was calculated first in Eq. 10. The square of K_{ik}, K_{ik}^2 then was required. T is the sum of corresponding trial index for all experimental values. P is T divided by the number of tests, called correction term.

$$K_{\mathrm{ik}} = \sum_{\mathrm{k=1}}^{3} y(n)_{\mathrm{ik}}, \tag{10}$$

W is the sum of the squares for all trial indexes, viz.

$$W = \sum_{\mathrm{n=1}}^{12} [y(n)]^2, \tag{11}$$

where S is the difference of W and P; S_{i} and Se are called efficacy square sum, the larger it is, the factor i has a greater effect on the trial index.

$$S_{\mathrm{i}} = \sum_{\mathrm{k=1}}^{3} K_{\mathrm{ik}}^2 - P\ ; \tag{12}$$

$$S_{\mathrm{e}} = S - \sum_{\mathrm{i=1}}^{4} S_{\mathrm{i}}, \tag{13}$$

where n is the degree of freedom, for each factor is 2 (SiO_2 is 3), it is the number of levels subtract 1. The degree of freedom for the entire experiment is 11, which is the number of all experiments subtracted by 1. So the degree of freedom for the error column is the degree of freedom for the entire experiment subtracting the degree of freedom for every factor, which is 2.

Mean square V is a criterion for the degree of importance, which is the efficacy square sum divides the degree of freedom, viz.

$$\mathrm{V} = S/n\ , \tag{14}$$

F is the mean square of each factor dividing the error column's mean square. According to mathematical statistics, F-test has three levels, which are 1 %, 5 %, 20 %. Two parameters, $N1$ and $N2$, in the F distribution table, $N1$ is the degree of freedom for factors, $N2$ is the degree of freedom for the error column. For example, while $N1$ = 3, $N2$ = 2, 5 %, the corresponding value in the F-test distribution is 19.2, which is written as $F_{0.05}(3,2)$ = 19.2. The F value of a factor, such as larger than the value on the 1 % F distribution critical value table, is particularly important, and shall be written as "※※". If between the value of 1 % and 5 % F table, is important, shall be written as "※". 5 % and 20 % is some effect, shall be written as "(※)", smaller than 20 % is nearly no effect.

$$F = \frac{V_{\mathrm{i}}}{V_{\mathrm{e}}}, \tag{15}$$

When the mean squares F were calculated, the influence of each component on the importance of different properties of the coating was obtained in Table 3.

3.2.2. Discussion of analysis results

From the extreme difference R_{i} in Table 3, for *WCA*, the most considerable influence on the hydrophobic property of these coatings is SiO_2. Considering the VA result demonstrated in Table 4, SiO_2 is also "particularly important". Just from EDA and VA, others have little effect. However, the range of ingredients for these 12 groups of $L_{12}(4^1\times3^3)$ orthogonal experiments were based on several previous experiments. This prepared work was not used in the analysis, and with the references referred to before, we can only confirm the SiO_2 is particularly important in the hydrophobic property. However, TiO_2; C and KH550 shall not be regarded as having no effect like the results of VA.

Table. 4. Results of F-test in VA

	SiO_2	TiO_2	C	KH550
WCA θ	Particularly important	Nearly no effect	Nearly no effect	Nearly no effect
Frost weight in standard condition d_{stand}	Some effect	Nearly no effect	Nearly no effect	Nearly no effect
Thermal conductivity λ_1	Some effect	Nearly no effect	Important	Some effect
WCA degradation $\Delta\theta$	Important	Important	Important	Some effect

For frost weight, the situation is quite similar with WCA in EDA, which is SiO_2 also has the most significant influence on it while others have little. However, from the VA result shown in Table 4, SiO_2 has "some effect" on frost weight, while others have no effect. Considering SiO_2 is particularly important on WCA, it can be regarded hydrophobic property that has some effect on frost resistance. From Fig. 7, the experiment results also showed that the WCA does not have a perfectly negative correlation with the frost weight. SiO_2 is most important for the hydrophobic property, frost resistance, and performance degradation. However, the solubility of SiO_2 in PTFE solution is limited.

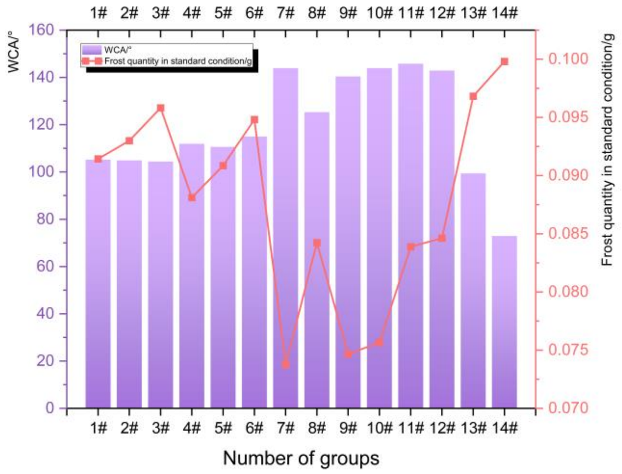

Fig. 7. The variation between WCA and frosting weight

More SiO_2 will cause a massive viscosity of the suspension and may be hard to stir. Graphite powder is essential to the heat transfer characteristic of the coating. TiO_2 and KH550 have some effect on the coating's performance degradation and heat transfer characteristics. Actually, according to our preliminary preparation experiment results, TiO_2 can be replaced by ZnO or Al_2O_3, KH560 can also replace KH550. The properties of the coating do not change significantly.

3.2.3. Visualized analysis

Fig. 8, at 6 min shows the formation of initial frost crystals on the frozen droplets, the initial frost crystals formed on the ice beads have four groups as irregular crystals, flake crystals, needle and pole crystals, and feather crystals 56, and the kind of crystal depended on the temperature of the surface from 248 – 273 K 57. At the beginning of the experiment, the surface was not thoroughly cooled, resulting in the surface frosting only appearing in the edge area, and the frosting was limited in the center area of the surface. Therefore, the frosting weight had little relationship with the WCA in this period.

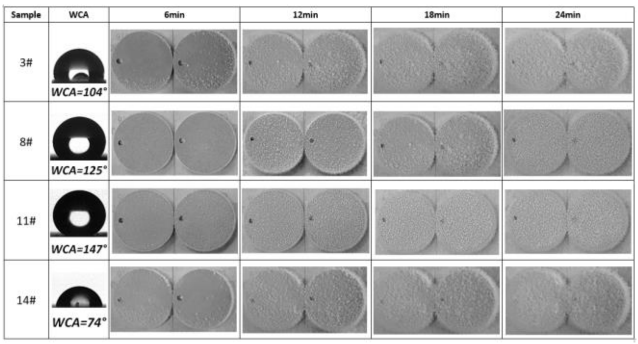

Fig. 8. Frost formation at different WCA

At 6 and 12 min, the frosting pattern on the hydrophobic surfaces was quite non-uniform and appeared "pock-marked" 26. Also, frost crystals were lower for samples 8 and 11#. At the edge of sheets, 4 groups all had a higher and more complete frost layer due to the edge effect 58. At 18 and 24 min, the process came to frost layer growth period and frost layer full growth period. In these two periods, the frost grew horizontally 59. The frost of 3 and 14# samples was fluffy while 8 and 11# is firm.

In Fig. 9, with the WCA improvement from 3# to 12#, the scanning electron microscope (SEM) shows that the surface morphology has a pitted structure of 1 – 10 μm size, which traps some amount of air.

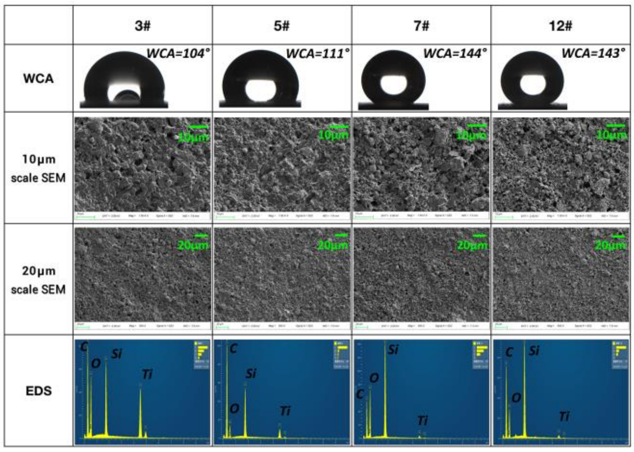

Fig. 9. SEM and EDS for 4 samples

These micrometer-scale pits enable water to hardly touch the surface. As a result, pit-like micrometer-scale structures covering the surface generated a high hydrophobicity. The roughness and WCA of the surface were increasing from 3# to 12# due to the size of pits becoming smaller because of more nanoscale solute in a gel. The energy dispersive spectrometer (EDS) demonstrates in Fig. 10 and reports that the WCA becomes higher with the increase of silicon content, which obey the analysis from extreme difference analysis and variance analysis in the last chapter.

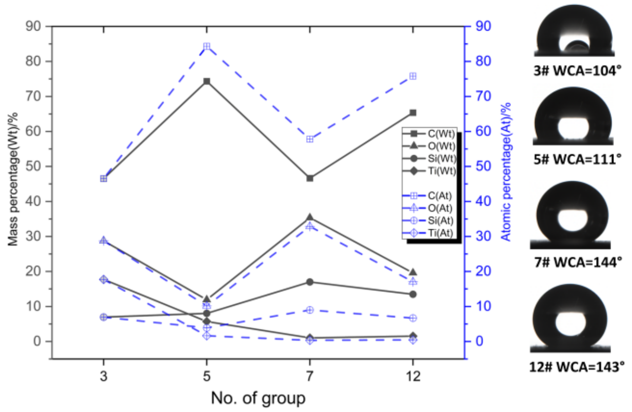

Fig. 10. Mass and atomic percentage from EDS for 4 samples

4. CONCLUSIONS

1. A PTFE hydrophobic frost retardation coating sprayed on evaporator surface with the first-step method was prepared, which is suitable for application in industry. The average water contact angle can reach 140°. Compared with the bare stainless substrate and pure

PTFE coating, the 15 min frost weight was reduced by 4.00 – 26.10 % and 2.00 – 22.89 %.
2. A method was developed to discuss coating properties using orthogonal experiments and statistical methods. Based on $L_{12}(4^1 \times 3^3)$ orthogonal experiment, extreme difference analysis and variance analysis were applied to investigate each ingredient on the properties of the coating. This analysis process can provide guidance for researchers who want to improve a particular property by modifying their coating composition without the chemical properties and morphology of the coating.
3. SiO_2 is particularly important on the hydrophobic property and has some effect on frost resistance. Other ingredients nearly do not affect these two properties.
4. The graphite powder is essential for the heat transfer characteristic of this coating, while SiO_2 and KH550 also have some effects. SiO_2, TiO_2 and graphite powder all have a significant effect, while KH550 had some effect on coating performance degradation.
5. A modification method for frost weight measurement under different temperature and humidity conditions was proposed in this paper to cope with the influence of the disunity for temperature and humidity conditions on the frost weight measurement. The relative error of frost weight measurement using this method is about 5 %.

Acknowledgments

This work was supported by National Key R&D Program of China(2020YFC1910100).

REFERENCES

1. **Sheng, W., Liu, P.P., Dang, C.B., Liu, G.X.** Review of Restraint Frost Method on Cold Surface *Renewable & Sustainable Energy Reviews* 79 2017: pp. 806 – 813. https://doi.org/10.1016/j.rser.2017.05.088
2. **Li, D., Chen, Z.Q., Shi, M.H.** Effect of Ultrasound on Frost Formation on a Cold Flat Surface in atmospheric air flow *Experimental Thermal and Fluid Science* 34 (8) 2010: pp. 1247 – 1252. https://doi.org/10.1016/j.expthermflusci.2010.05.005
3. **Song, M.J., Dand, C.B.** Review on the Measurement and Calculation of Frost Characteristics *International Journal of Heat and Mass Transfer* 124 2018: pp. 586 – 614. https://doi.org/10.1016/j.ijheatmasstransfer.2018.03.094
4. **Shen, J., Lu, K.L., Li, H.J.** Experimental Research on Defrosting Process of Cooling Fan with Heat Insulation Defrosting Device *Journal of Refrigeration* 35 (04) 2014: pp. 104 – 107. https://doi.org/10.3969/j.issn.0253-4339.2014.04.104
5. **Qiu, T., Feng, Y.H., Liu, Q.M., Li, C.Z., Du, P.** Investigation of Defrosting Control Function Based on Model and Sequence Diagram *Building Services Engineering Research & Technology* 36 (1) 2015: pp. 5 – 17. https://doi.org/10.1177/0143624414532931
6. **Wang, Z.Y., Wang, X.M., Dong, Z.M.** Defrost Improvement by Heat Pump Refrigerant Charge Compensating *Applied Energy* 85 (11) 2008: pp. 1050 – 1059. https://doi.org/10.1016/j.apenergy.2008.02.020
7. **Badri, D., Toublanc, C., Rouaud, O., Havet, M.** Review on Frosting, Defrosting and Frost Management Techniques in Industrial Food Freezers *Renewable and Sustainable Energy Reviews* 151 2021: pp. 1 – 20. https://doi.org/10.1016/j.rser.2021.111545
8. **Kim, M.H., Kim, H., Lee, K.S, Kim, D.P.** Frosting Characteristics on Hydrophobic and Superhydrophobic Surfaces: A review *Energy Conversion & Management* 2017: pp. 1 – 11. https://doi.org/10.1016/j.encoriman.2017.01.067
9. **Kwak, K., Bai, C.** A Study on the Performance Enhancement of Heat Pump Using Electric Heater Under the Frosting Condition: Heat Pump Under Frosting Condition *Applied Thermal Engineering* 30 (6 – 7) 2010: pp. 539 – 543. https://doi.org/10.1016/j.applthermaleng.2009.10.016
10. **Wang, F.H., Wang, Z.H., Zheng, Y., Lin, Z., Hao, P.F., Huan, C., Wang, T.** Performance Investigation of a Novel Frost-free Air-source Heat Pump Water Heater Combined with Energy Storage and Dehumidification *Applied Energy* 139 2015: pp. 212 – 219. https://doi.org/10.1016/j.apenergy.2014.11.018
11. **Li, Z., Hihara, E., Saikawa, M.** Combination of Air-source Heat Pumps With Liquid Desiccant Dehumidification of Air *Energy Conversion & Management* 57 2012: pp. 107 – 116. https://doi.org/10.1016/j.enconman.2011.12.023
12. **Wang, C.C., Huang, R.T., Sheu, W.J., Chang, Y.J.** Some Observations of the Frost Formation in Free Convection: with and without the Presence of Electric Field *International Journal of Heat & Mass Transfer* 47 (14/16) 2004: pp. 3491 – 3505. https://doi.org/10.1016/j.ijheawwtmasstransfer.2003.12.021
13. **Qin, Y., Dong, B., Li, W.** Experimental Study of the Frosting Characteristic of Water on a Cold Surface in the Magnetic Field *Experimental Thermal and Fluid Science* 114 (1) 2020: pp. 1 – 31. https://doi.org/10.1016/j.expthermflusci.2020.110044
14. **Sheikholeslami, M., Gorjibandpy, M., Ganji, D.D.** Review of Heat Transfer Enhancement Methods: Focus on Passive Methods Using Swirl Flow Devices *Renewable & Sustainable Energy Reviews* 49 2015: pp. 444 – 469. https://doi.org/10.1016/j.rser.2015.04.113
15. **Sommers, A.D., Jacobi, A.M.** Air-side Heat Transfer Enhancement of a Refrigerator Evaporator Using Vortex Generation *International Journal of Refrigeration* 28 (7) 2005: pp. 1006 – 1017. https://doi.org/10.1016/j.ijrefrig.2005.04.003
16. **Yan, W.M., Li, H.Y., Tsay, Y.L.** Thermofluid Characteristics of Frosted Finned-tube Heat Exchangers *International Journal of Heat & Mass Transfer* 48 (15) 2005: pp. 3073 – 3080. https://doi.org/10.1016/j.ijheatmasstransfer.2005.02.018
17. **Yang, D.K., Lee, K.S., Song, S.** Fin Spacing Optimization of a Fin-tube Heat Exchanger Under Frosting Conditions *International Journal of Heat & Mass Transfer* 49 (15/16) 2006: pp. 2619 – 2625. https://doi.org/10.1016/j.ijheatmasstransfer.2006.01.016
18. **Zhang, P., Lv, F.Y.** A Review of the Recent Advances in Superhydrophobic Surfaces and the Emerging Energy-related Applications *Energy* 82 2015: pp. 1068 – 1087. https://doi.org/10.1016/j.energy.2015.01.061
19. **Song, M.J., Deng, S.M., Dang, C.B., Mao, N., Wang, Z.H.** Review on Improvement for Air Source Heat Pump Units during Frosting and Defrosting *Applied Energy* 211 2018: pp. 1150 – 1170. https://doi.org/10.1016/j.apenergy.2017.12.022
20. **Kim, M.H., Kim, H., Lee, K.S., Kim, D.P.** Frosting Characteristics on Hydrophobic and Superhydrophobic

Surfaces: A Review *Energy Conversion and Management* 138 2017: pp. 1 – 11. https://doi.org/10.1016/10.1016/j.encoriman.2017.01.067

21. **Mohammed, A., Wang, C.C.** Review of Defrosting Methods *Renewable and Sustainable Energy Reviews* 73 2017: pp. 53 – 74. https://doi.org/10.1016/j.rser.2017.01.120
22. **Mishchenko, L., Hatton, B., Bahadur, V., Taylor, J.A., Krupenkin, T., Aizenberg, J.** Design of Ice-free Nanostructured Surfaces Based on Repulsion of Impacting Water Droplets *Acs Nano* 4 (12) 2010: pp. 7699 – 707. https://doi.org/10.1021/nn102557p
23. **Hou, Y., Yu, M., Shang, Y., Zhou, P., Song, R.Y., Xu, X.N., Chen, X.M, Wang, Z.K., Yao, S.H.** Suppressing Ice Nucleation of Supercooled Condensate with Biphilic Topography *Physical Review Letters* 120 (7) 2018: pp. 075902.1 – 075902.6. https://doi.org/10.1103/PhysRevLett.120.075902
24. **Rahman, M.A., Jacobi, A.M.** Experimental Study on Frosting/Defrosting Characteristics of Microgrooved Metal Surfaces *International Journal of Refrigeration* 50 2015: pp. 44 – 56. https://doi.org/10.1016/j.ijrefrig.2014.11.002
25. **Na, B., Webb, R.L.** A Fundamental Understanding of Factors Affecting Frost Nucleation *International Journal of Heat & Mass Transfer* 46 (20) 2003: pp. 3797 – 3808. https://doi.org/10.1016/S0017-9310(03)00194-7
26. **Wu, X.M., Webb, R.L.** Investigation of the Possibility of Frost Release from a Cold Surface *Experimental Thermal and Fluid Science* 24 (3 – 4) 2001: pp. 151 – 156. https://doi.org/10.1016/S0894-1777(01)00045-0
27. **Kim, A., Lee, C., Kim, H., Kim, J.** Simple Approach to Superhydrophobic Nanostructured Al for Practical Antifrosting Application Based on Enhanced Self-propelled Jumping Droplets *ACS Applied Materials & Interfaces* 13 (7) 2015: pp. 7206 – 7213. https://doi.org/10.1021/acsami.5b00292
28. **Kulinich, S.A., Farhadi, S., Nose, K., Du, X.W.** Superhydrophobic Surfaces: Are They Really Ice-Repellent? *Langmuir* 27 (1) 2011: pp. 25 – 29. https://doi.org/10.1021/la104277q
29. **Muthiah, P., Hsu, S., Sigmund, W.** Coaxially Electrospun PVDF-Teflon AF and Teflon AF-PVDF Core-Sheath Nanofiber Mats with Superhydrophobic Properties *Langmuir* 26 (15) 2010: pp. 12483 – 12487. https://doi.org/10.1021/la100748g
30. **Qiu, C., Li, M., Chen, S.** Anti-Icing Characteristics of PTFE Super Hydrophobic Coating on Titanium Alloy Surface *Journal of Alloys and Compounds* 860 (S1) 2020: pp. 157907. https://doi.org/10.1016/j.jallcom.2020.157907
31. **Chi, F.T., Liu, D.J., Wu, H.Y., Lei, J.H.** Mechanically Robust and Self-cleaning Antireflection Coatings From Nanoscale Binding of Hydrophobic Silica Nanoparticles *Solar Energy Materials and Solar Cells* 200 2019: pp. 1 – 8. https://doi.org/10.1016/j.solmat.2019.109939
32. **Xia, B.B., Luo, J.H., Li, Y.Y., Yang, B.W., Zhang, S.M., Jiang, B.** Preparation of Sponge-like Porous SiO_2 Antireflective Coatings with Excellent Environment-Resistance by an Acid-catalysed Sol–gel Method *RSC Advances* 7 (43) 2017: pp. 26834 – 26838. https://doi.org/10.1039/c7ra00622e
33. **Ye, L.Q., Zhang, Y.L., Zhang, X.X., Hu, T., Ji, R., Ding, B., Jiang, B.** Sol-gel Preparation of SiO2/TiO2/SiO2–TiO2 Broadband Antireflective Coating for Solar Cell Cover Glass *Solar Energy Materials and Solar Cells* 111 2013: pp. 160 – 164. https://doi.org/10.1016/j.solmat.2012.12.037
34. **Han, K., Kim, J.H.** Fabrication of TiO2/SiO2 Multilayer Film Structure by the Sol-gel Process with Efficient Thermal Treatment Methods *Applied Surface Science* 263 2012: pp. 69 – 72. https://doi.org/10.1016/j.apsusc.2012.08.123
35. **Sermon, P.A., Leadley, J.G.** Fluoroalkylsilane Modification of Sol–Gel SiO2-TiO2 Coatings *Journal of Sol-Gel Science and Technology* 32 (1 – 3) 2004: pp. 293 – 296. https://doi.org/10.1007/s10971-004-5805-5
36. **Mazloum, A., Jaroslav, K., Emmer, Š., Sevostianov, I.** Copper–graphite Composites: Thermal Expansion, Thermal and Electrical Conductivities, and Cross-property Connections *Journal of Materials Science* 2016: pp. 1 – 13. https://doi.org/10.1007/s10853-016-0067-5
37. **Wang, K., Wu, J.Y., Wang, R.Z.** Thermal Conductivity Measurement of the CaCl_2/Expanded Graphite Compound Asorbent *Journal of Shanghai Jiaotong University* 42 (1) 2008: pp. 106 – 109. https://doi.org/10.3321/j.issn:1006-2467.2008.01.023
38. **Chen, Y.C, Lin, H.C., Lee, Y.D.** The Effects of Filler Content and Size on the Properties of PTFE/SiO_2 Composites *Journal of Polymer Research* 10 (4) 2003: pp. 247 – 258. https://doi.org/10.1023/B:JPOL.0000004620.71900.16
39. **You, Y., Yuan, Y.** Influences of Compound Coupling Agent on Properties of SiO_2/Polytetrafluoroethylene Composites *Fuhe Cailiao Xuebao/Acta Materiae Compositae Sinica* 32 (2) 2015: pp. 465 – 470. https://doi.org/10.13801/j.cnki.fhclxb.20140509.002
40. **Yuan, Y., Yin, Y.T, Yu, D.D., Lin, H.D., Wang, J., Tang, B., Li, E.Z.** Effects of Compound Coupling Agents on the Properties of PTFE/SiO2 Microwave Composites *Journal of Materials Science Materials in Electronics* 28 (4) 2016: pp. 1 – 8. https://doi.org/10.1007/s10854-016-5929-8
41. **Yuan, Y., Lin, H.D., Yu, D.D., Yin, Y.T., Tang, B., Li, E.Z., Zhang, S.R.** Effects of Perfluorooctyltriethoxysilane Coupling Agent on the Properties of Silica Filled PTFE Composites *Journal of Materials Science: Materials in Electronics* 28 (12) 2017: pp. 8810 – 8817. https://doi.org/10.1007/s10854-017-6608-0
42. **Chen, P., Kou, K.C., Jia, Q., Zhang, Y., Wu, G.L., Ji, T.Z.** Improved Thermal Conductivity and Dielectric Properties of HBN/PTFE Composites via Surface Treatment by Silane Coupling Agent *Composites Part B Engineering* 111 2016: pp. 83 – 90. https://doi.org/10.1016/j.compositesb.2016.11.050
43. **Oberli, L., Caruso, D., Hall, C., Fabretto, M., Murphy, P.J., Evans, D.** Condensation and Freezing of Droplets on Superhydrophobic Surfaces *Advances in Colloid & Interface Science* 210 2014: pp. 47 – 57. https://doi.org/10.1016/j.cis.2013.10.018
44. **Nath, S., Boreyko, J.B.** On Localized Vapor Pressure Gradients Governing Condensation and Frost Phenomena *Langmuir: The ACS Journal of Surfaces and Colloids* 2016: pp. 1 – 50. https://doi.org/10.1016/10.1021/acs.langmuir.6b01488
45. **Huang, L.Y., Liu, Z.L., Liu, Y.M., Gou, Y.J.** Preparation and Anti-frosting Performance of Super-hydrophobic Surface Based on Copper Foil *International Journal of Thermal Sciences* 50 (4) 2011: pp. 432 – 439. https://doi.org/10.1016/j.ijthermalsci.2010.11.011

46. **Kim, S., Kim, K.** Dropwise Condensation Modeling Suitable for Superhydrophobic Surfaces *Journal of heat transfer: Transactions of the ASME* 2011 (8) 2011: pp. 081502-1 – 081502-8. https://doi.org/10.1115/1.4003742

47. **Wang, H., Liu, Y.W., Yang, P., Wu, R.J., He, Y.L.** Parametric Study and Optimization of H-type Finned Tube Heat Exchangers Using Taguchi Method *Applied Thermal Engineering* 2016: pp. 128 – 138. https://doi.org/10.1016/j.applthermaleng.2016.03.033

48. **Zhou, W.Y., Liu, W.B., Wang, Y., Lyu, X.Y., Yang, L.** Analysis of Influencing Factors on NOx emission in Gas-Fired Heating and Hot Water Combi-Boilers Based on Orthogonal Method *Journal of Thermal Science* 30 (3) 2021: pp. 1088 – 1095. https://doi.org/10.1007/s11630-020-1329-8

49. **Shen, W.D., Tong, J.G.** Thermodynamics an Engineering Approach (5th edition) *Higher Education Press* China, 2016.

50. **Badri, D., Toublanc, C., Rouaud, O., Havet, M.** Review on Frosting, Defrosting and Frost Management Techniques in Industrial Food Freezers *Renewable and Sustainable Energy Reviews* 151 2021: pp. 1 – 20. https://doi.org/10.1016/J.RSER.2021.111545

51. **Holman, J.P.** Heat Transfer (10th edition) *McGraw-Hill Companies Inc* America, 2010.

52. **Yin, H.J., Yang, Z., Chen, A.Q., Zhang, N.** Experimental Research on a Novel Cold Storage Defrost Method Based on Air Bypass Circulation and Electric Heater *Energy* 37 (1) 2012: pp. 623 – 631. https://doi.org/10.1016/j.energy.2011.10.040

53. **Melo, C., Knabben, F.T., Pereira, P.V.** An Experimental Study on Defrost Heaters Applied to Frost-free Household Refrigerators *Applied Thermal Engineering* 51 (1 – 2) 2013: pp. 239 – 245. https://doi.org/10.1016/j.applthermaleng.2012.08.044

54. **Department of Probability and Statistics**, Institute of Mathematics. Orthogonal experimental design *Chinese Academy of Sciences* China, 1970.

55. **Gao, Y.** Orthogonal and Regression Experimental Design Methods *Metallurgical Industry Press* China, 1988.

56. **Wu, X.M., Dai, W.T., Xu, W.F., Tang, L.M.** Mesoscale Investigation of Frost Formation on a Cold Surface *Experimental Thermal & Fluid Science* 31 (8) 2007: pp. 1043 – 1048. https://doi.org/10.1016/j.expthermflusci.2006.11.002

57. **Sahin, A.Z.** Effective Thermal Conductivity of Frost During the Crystal Growth Period *International Journal of Heat & Mass Transfer* 43 (4) 2000: pp. 539 – 553. https://doi.org/10.1016/S0017-9310(99)00162-3

58. **Liu, Z.L., Wang, H.Y., Zhang, X.H., Meng, S., Ma, C.F.** An Experimental Study on Minimizing Frost Deposition on a Cold Surface under Natural Convection Conditions by Use of a Novel Anti-frosting Paint. Part II Long-term Performance, Frost Layer Observation and Mechanism Analysis *International Journal of Refrigeration* 29 (2) 2006: pp. 237 – 242. https://doi.org/10.1016/j.ijrefrig.2005.05.018

59. **Song, M.J., Dang, C.B., Tomohira, H., Eiji, H.** Review of Experimental Data Associated with the Solidification Characteristics of Water Droplets on a Cold Plate Surface at the Early Frosting Stage *Energy and Buildings* 223 2020: pp. 1 – 53. https://doi.org/10.1016/j.enbuild.2020.110103